17th Australasian Fluid Mechanics Conference
Auckland, New Zealand
5-9 December 2010

Constant adverse pressure gradient turbulent boundary layers

Z. Harun, J. P. Monty, I. Marusic

Department of Mechanical and Manufacturing
University of Melbourne, Melbourne 3010, Australia

Abstract

Significant progress has been made towards understanding the large scale features of wall-bounded shear flow in zero pressure gradient (ZPG) turbulent boundary layers (TBL). Here we consider their effects in adverse pressure gradient (APG) flows where the pressure gradient parameter is held constant and Reynolds number is varied. This is done by documenting the changes in the mean velocity, streamwise turbulence intensities and their associated spectral densities. Increased large-scale activity near the wall is seen with increasing Reynolds number and for this pressure gradient, the mean flow deviates from the classically regarded log-law.

Introduction

The case of the adverse pressure gradient boundary layer is of great importance since this must be the condition of a boundary layer prior to separation. As such, many boundary layer control strategies will be designed for implementation in APG conditions.

While there are some features of APG boundary layers that are well-known, such as the stronger wake of the mean velocity profile and increased broadband turbulence intensity, $\overline{u^2}/U_\tau^2$ in the logarithmic and wake region, there remain important features to be investigated. The large-scale structure of the flow is a case in point. Compared with the ZPG case, there is far less known about the large-scale features in APG boundary layers. This may be due, in part, to the greater number of variables pertinent to the APG case. In order to reduce the parameter space, the present investigation presents data with varying Reynolds numbers, $Re_\tau = \delta U_\tau/\nu$ (where δ is the boundary layer thickness, U_τ is the friction velocity and ν is the kinematic viscosity) and fixed pressure gradient parameter

$$\beta = \frac{\delta^*}{\tau_o}\frac{dP}{dx} \tag{1}$$

where δ^* is displacement thickness and τ_o is wall shear stress, P is static pressure and x is streamwise distance. The authors are not aware of a previous study maintaing constant β with varying Reynolds number. It should be noted that this is a complementary study to that of Harun *et al* [5], where a series of experiments were conducted at fixed Reynolds number ($Re_\tau \approx 1800$) and varying β.

Harun *et al* [5] noted a significant difference between the mean velocity of APG and ZPG flows; as the APG strength increased, a change of κ and A in the log-law of the wall was observed. It was also found that there is a change in the 'outer peak' in the energy spectra, both in location and length-scale from z/δ = 0.06 and λ_x/δ = 6 in ZPG flow [6] to z/δ = 0.3 and $\lambda_x/\delta \approx 2$ in the strong APG flow. The present study aims to build on this previous work to understand the effect of increasing Reynolds number on the large-scale structure of a strong, fixed, adverse pressure gradient boundary layer.

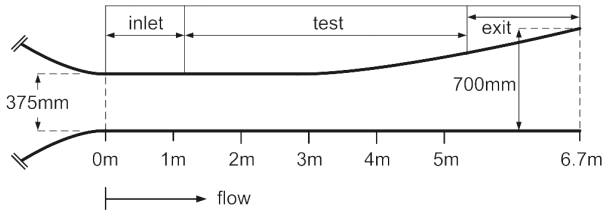

Figure 1: Wind tunnel general geometries

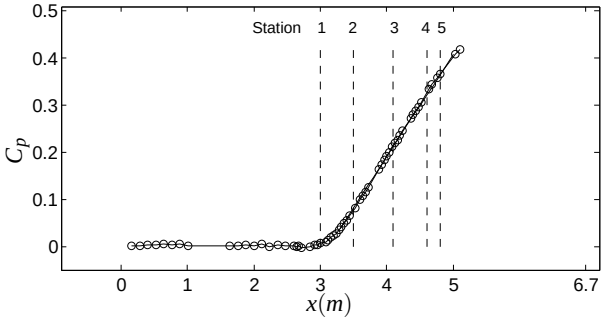

Figure 2: Coefficient of pressure C_p

Experimental set up

Facility

The experiments were performed in an open-return blower wind tunnel. The important features of the tunnel are a settling chamber containing honeycomb and five screens followed by a contraction with area ratio of 8.9:1 which leads into an initial inlet section area of 940 mm wide by 375 mm. The test section has a an adjustable roof made from acrylic. It has a length of 4.2 m. The sections heights are 375 mm at the trip wire (x = 0 m), 400 mm at x = 3 m and 550 mm at x = 5 m. The geometry is shown in figure 1. The wind tunnel is divided into four sections, the inlet, the ZPG, APG and outlet sections. The pressure gradient was carefully adjusted so that the coefficient of pressure C_p was set to be within ± 0.01 throughout the inlet velocities tested. Figure 2 shows C_p plotted against streamwise position. The first 8 pressure taps are in the inlet section. The figure shows that the next 15 pressure taps were in ZPG. This is to ensure that the flow was stable before any pressure gradient is introduced.

Oil Film Interferometry

The method of Oil Film Interferometry, OFI was used independently to determine the skin friction coefficient C_f. It was noted that C_f from Clauser chart and Preston tube in an APG study carried out with the same wind tunnel used by Marusic and Perry (1995) [10] differ by 2% for $1000 < Re_\tau < 3500$.

OFI measurements took place at the same location that the hot-wire anemometer measurements had been performed. A 30 cSt Dow Corning 200 Fluid, a silicon based oil was dropped onto a glass plug, flush-fit to the wind tunnel wall. Temperature and pressure were measured while pictures of fringes on the droplet

were taken. Wall shear is obtained through

$$\tau_w = \mu_{oil}\left(\frac{\Delta x}{\Delta t}\right)\frac{2\sqrt{n_{oil}^2 - n_{air}^2 sin^2\theta}}{\lambda}, \qquad (2)$$

θ is the illumination incident angle, n_{air} and n_{oil} are refractive indices of air and oil and λ is the wavelength of the light source (λ = 589.9 nm for the sodium lamp used). Δx is the fringe displacement found using Huang Hilbert Transform (HHT) method discussed by Chauhan *et al* [2] and Δt is the time. More about the OFI method, background and calibration can be found in Ng *et al* [13].

Experimental parameters

All of the measurements were performed using single hot-wire anemometry. The hot-wire probes were all operated in constant temperature mode using an AA Lab Systems AN-1003 anemometer with overheat ratio of 1.8 and the system had a frequency response of at least 50 kHz. A Dantec probe support (55H20) was used. Wollaston wires of diameter ϕ = 2.5 μm are soldered to the prong tips and etched to give a platinum filament of the desired length, l.

Since the experiment required measurement at different Reynolds numbers, the dimensionless wire length l^+ would change as l^+ is proportional to U_τ, the friction velocity, if the exposed wire length l was maintained ($l^+ = lU_\tau/\nu$). l^+ should be as small as possible to reduce spatial resolution problems. For this experiment, we have chosen l^+=16 $\pm$ 1.

In table 1, U_1 is the free-stream velocity, U_τ is the friction velocity by Oil Film Interferometry (OFI). Superscript '+' is used to denote viscous scaling e.g. $z^+ = zU_\tau/\nu$, $U^+ = U/U_\tau$, $t^+ = tU_\tau{}^2/\nu$. The Reynolds number, Re_τ (Kármán number) is given by $\delta U_\tau/\nu$, where δ is the boundary layer thickness determined from a modified Coles law of the wall/wake fit to the mean velocity profile (Jones *et al* [8]). $t^+ = tU_\tau{}^2/\nu$ is the non-dimensionalised sample interval, where $t = 1/f_s$, f_s is sampling rate. All experimental parameters are shown in table 1.

Results

Coefficient of friction

Since the friction velocity requires measurement of the wall shear stress, it is critical that this quantity is measured as accurately as possible. Figure 3 shows the coefficient of friction plotted as a function of Re_τ. It shows that there is almost a constant shift between C_f measured by OFI compared to C_f determined from the Clauser method, with a percentage difference of approximately 10 – 15%. In this paper we will use U_τ determined from wall shear stress measured by OFI, since it is uncertain whether the classical log-law of the wall, on which the Clauser method relies, remains valid in strong APG flows.

Mean velocity and broadband turbulence intensity profiles

Figure 4(a) displays the mean velocity profiles for $\beta \approx 4.4$. The mean velocity profiles collapse in the inner region for all Reynolds numbers. The constants κ and A in the log-law of the wall equation $U^+ = \kappa^{-1}\ln(z^+) + A$, are determined from a linear fit to the traditional logarithmic region of the mean velocity profile defined as $70 < z^+ < 0.15Re_\tau$. The curve-fit yields an average value of κ = 0.36 and A = 2.2. The classical log-law with constants κ = 0.41, A = 5.0 is shown for comparison. Clearly the APG data lie below the classical log-law. Deviation from the log-law of the wall has been documented [11, 9]. Measurements performed at a constant Reynolds number with variable β showed a gradual downward shift of the mean velocity profiles in the traditional log region as the strength of the APG was increased [5].

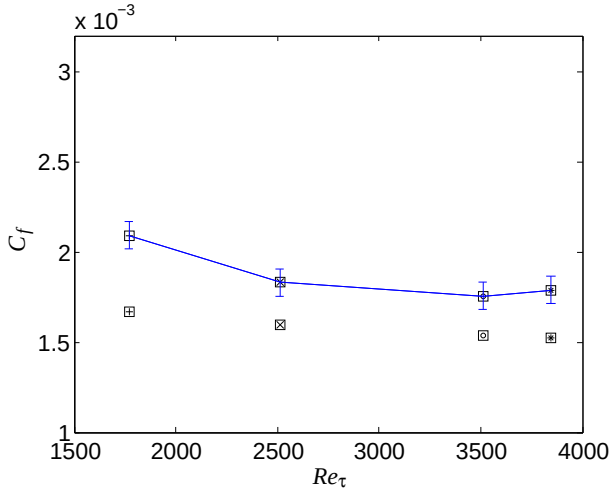

Figure 3: Coefficient of friction, C_f for constant $\beta \approx$4.4. C_f obtained from OFI. The error bars are of magnitude $\pm$2.5%. C_f obtained from Clauser chart are the lower symbols shown in Table 1.

In this study, having constant $\beta \approx 4.4$, it appears that it is solely pressure gradient that causes deviation from the log-law of the wall and not the Reynolds number. Note that Reynolds number has been increased from $Re_\tau \approx 1700$ to $Re_\tau \approx 3800$. However, the Reynolds number range is relatively small, so higher Reynolds number studies should be carried out to confirm this result.

Figure 4(b) shows the broadband turbulence intensity profiles. At z^+ = 15, $\overline{u^2}/U_\tau^2$ maintains a similar magnitude ($\approx$ 9) as Reynolds number increases. The higher Reynolds number data appear to collapse through most of the flow, well into the outer region, while the lower Reynolds number intensity is slightly lower in magnitude beyond z^+ = 15. This result suggests that there may be only slight differences in the structure of the flow with increasing Reynolds number.

Energy spectra

Pre-multiplied energy spectra, $k_x\phi_{uu}$ will be plotted against streamwise wavelength $\lambda_x = 2\pi/k_x$, where ϕ_{uu} is the spectral density of the streamwise velocity fluctuations, $k_x = 2\pi f/U_c$ is the streamwise wavenumber, f is the frequency and U_c is the convection velocity. In ZPG flow, there is a highly energetic peak in the near wall region occurring at $z^+ \approx$15 and $\lambda_x{}^+ \approx$ 1000 referred to as the inner peak'. The inner peak is due to the near wall cycle of streaks and quasi-streamwise vortices. Further from the wall, [6] showed that there is a second peak in the boundary layer spectra map at $z \approx 0.06\delta$ corresponding to superstructures of wavelength $\lambda_x \approx 6\delta$. These features can be seen in figure 6 which displays coloured contours of $k_x\phi_{uu}$ against streamwise wavelength and wall-distance (the 'spectra map') for a lower Reynolds number ZPG case.

Figures 5(a) to (d) display energy spectra maps for the strong APG case with matched β. As Re_τ increases from 1700 to 2500, $k_x\phi_{uu}/U_\tau^2$ increases in the outer region (as does $\overline{u^2}/U_\tau{}^2$). For higher Reynolds number, the spectra maps look very similar. Observing the peak energy (deep red contours) in the outer region, it appears that, at the same pressure gradient, a shift

Symbol	U_1 m/s	x m	Re_τ	δ m	δ^*	θ	Π	β	P^+ x10^{-3}	ν/U_τ μm	d μm	l^+	t^+	TU_1/δ
⊞	8.01	4.8	1740	0.108	0.0248	0.0156	2.35	4.39	-34.7	62.1	2.5	15	0.08	18000
⊠	12.89	4.8	2500	0.100	0.0225	0.0143	2.44	4.40	-21.8	40.8	2.5	16	0.19	16000
⊡	17.10	4.8	3510	0.105	0.0225	0.0147	2.25	4.53	-15.9	30.3	2.5	16	0.34	19600
⊛	19.13	4.8	3850	0.102	0.0222	0.0145	2.31	4.40	-14.4	27.2	2.5	16	0.42	24200
▷	14.24	3.0	1830	0.052	0.0074	0.0055	0.65	ZPG	ZPG	28.7	2.5	17	0.38	21800

Table 1: Experimental parameters for hotwire experiments with constant β.

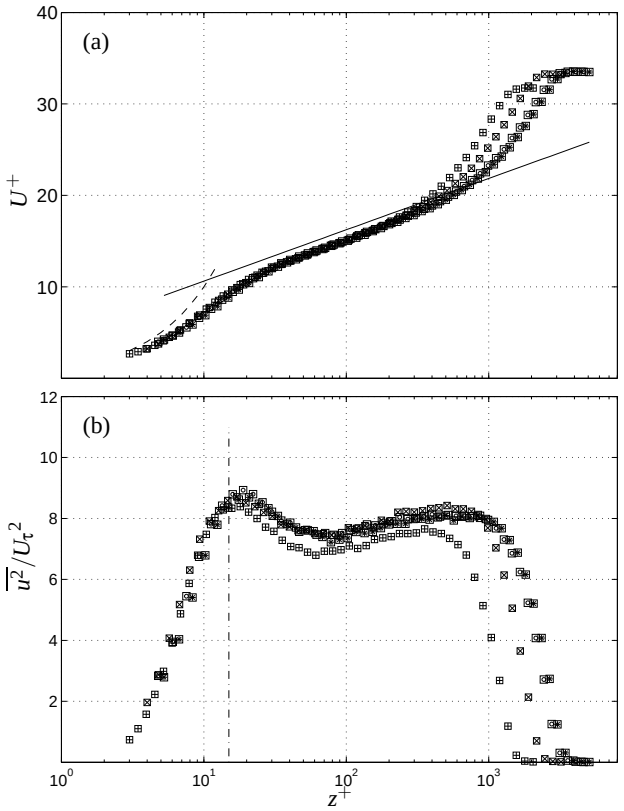

Figure 4: Statistics of the APG boundary layer for $\beta \approx 4.4$ with increasing Re_τ (a) Mean velocity; (b) Broadband turbulence intensity. For symbols, refer to table 1. The solid line shows $U^+ = \kappa^{-1}\ln(z^+) + A$, $\kappa = 0.41$ and $A = 5$, while the dashed line shows $U^+ = y^+$ and the dashed-dot line indiecates $z^+ = 15$.

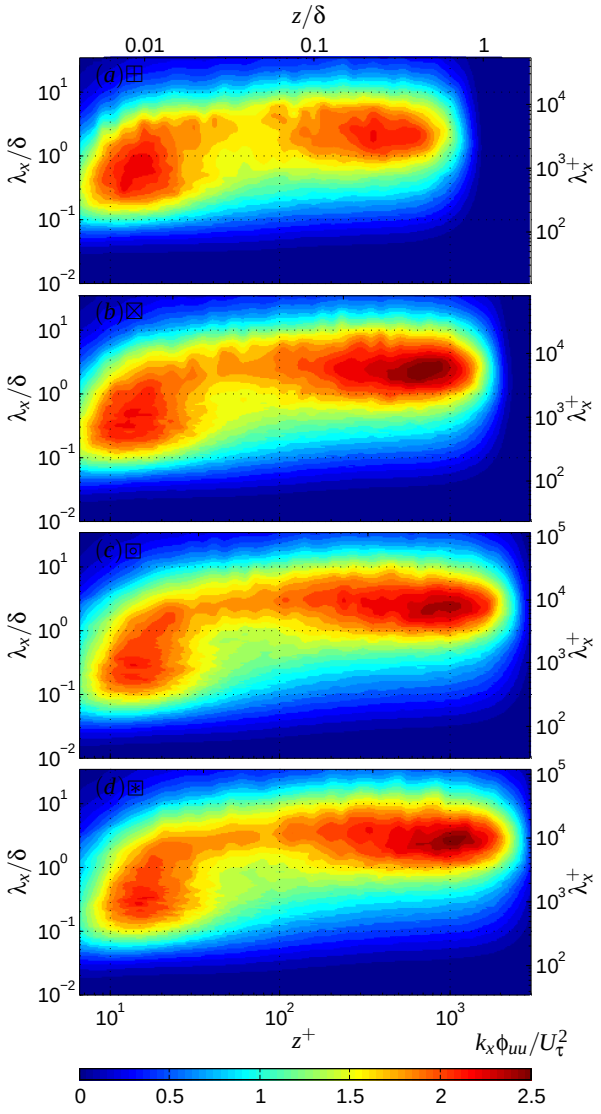

Figure 5: Pre-multiplied energy spectra of streamwise velocity, $k_x\phi_{uu}/U_\tau^2$ constant β. For detail, refer to Table 1.

toward larger length-scales with Re_τ increasing can be seen, although it is only weak. Perhaps the most notable result is the strength of the large-scale structures in the outer region of APG flows compared with ZPG (comparing figure 6 with 5).

For a more detailed comparison, energy spectra at specific locations are plotted in figures 7(a) – (d). At $z^+ \approx 15$ there appear to be only small changes in the spectra with Re_τ, except at the lower Re_τ, where the large-scales are slightly less energetic.

At $z^+ \approx 100$, $k_x\phi_{uu}/U_\tau^2$ increases markedly from $Re_\tau = 1700$ to 2500, yet there appears little change with further increase of Reynolds number. At the higher Reynolds numbers, the large-scale energy is much stronger and the peak energy occurs at the significantly longer wavelength of $\lambda_x/\delta \approx 2$ - 3.

At $z^+ \approx (15Re)^{0.5}$ (the midpoint of the logarithmic region) and $z/\delta \approx 0.3$, the peak energy occurs at $\lambda_x/\delta \approx 1$ for the lowest Reynolds number. However, as the Reynolds number is increased, the peak energy shifts to longer wavelengths to $\lambda_x/\delta \approx 2$ - 3 as shown in shown in figure 7(c and d). It could be argued that the large-scale energy becomes slightly stronger and shifts to slightly longer wavelengths with increasing Re_τ.

In summary,the lower Re_τ (1740) appears to differ from the

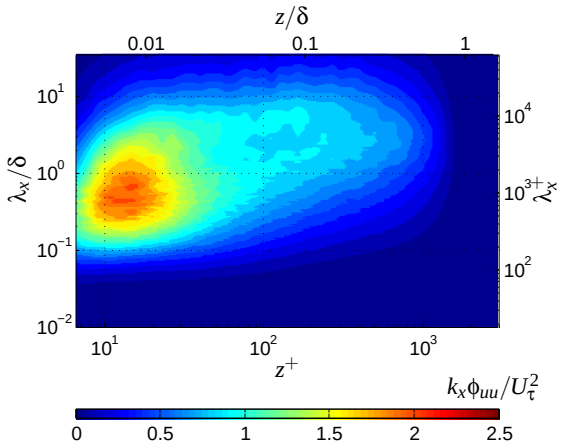

Figure 6: Pre-multiplied energy spectra of streamwise velocity, $k_x\phi_{uu}/U_\tau^2$ for ZPG at Re_τ 1850. For detail, refer to Table 1.

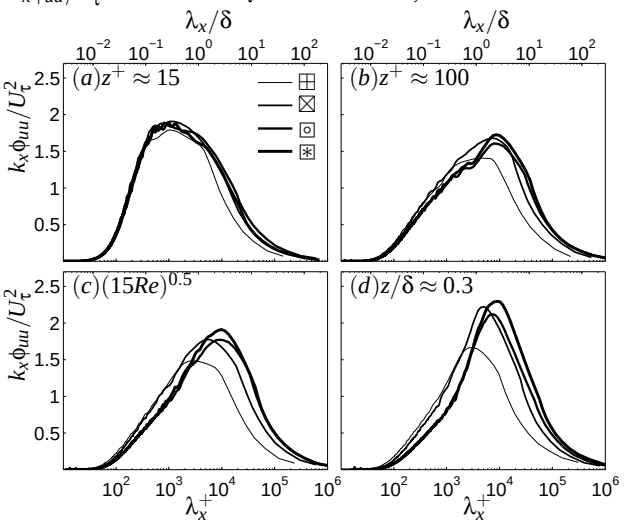

Figure 7: Pre-multiplied energy spectra of streamwise velocity fluctuation $k_x\phi_{uu}/U_\tau^2$ constant β at selected heights from the wall. Re_τ increases with line in increasing thickness.

higher Re_τ cases in the large scale contribution to the energy spectra. This may indicate that the separation of scales is insufficient at this Reynolds number. Therefore, it could be recommended that $Re_\tau \approx 2000$ represents a lower limit for a strong APG boundary layer to be classified as 'high' Reynolds number.

Conclusions

The mean velocity profiles for APG turbulent boundary layers deviates from the classical log-law of the wall. There is a downward shift in the logarithmic region observed in strong pressure gradients of $\beta \approx 4.4$. Based on the constant Re_τ data with increasing β, the downward shift is gradual as β increases. Thus we can confirm that β is the sole factor affecting the deviation from the log-law while it is insensitive to Re_τ, at least for the range of experiments presented here.

The broadband turbulence intensity profiles collapse in the inner region for all Reynolds number data except for the lowest Re_τ (1740). The turbulence intensity is higher in the outer region and significantly different in shape compared to ZPG.

Through an energy spectra analysis, the outer region is clearly affected by APG as compared to ZPG [5]. Even though broadband turbulence intensity $\overline{u^2}/U_\tau^2$ in the inner and outer regions are approximately of the same magnitude for higher Re_τ, there appears to be a weakly increasing contribution from larger scales, starting in the logarithmic region and continuing into the outer region. In ZPG flow, the outer peak in energy spectra grows weakly in magnitude with Reynolds number [6]. In the strong adverse pressure gradient case studied here, it is also evident that larger scales structures increase in strength as Re_τ increases, consistent with ZPG. However, data at higher Reynolds numbers are required to confirm this result.

References

[1] Bourassa, C. and Thomas, F.O., An experimental investigation of a highly accelerated turbulent boundary layer, *J. Fluid Mech.*, **634**, 2009, 359–404.

[2] Chauhan, K., Ng, H., and Marusic, I., Analysis of oil film interferograms for wall-shear stress measurements using Hilbert-Huang transform, *Under consideration*

[3] Clauser, F.H., Turbulent boundary layer in adverse pressure gradient, *J. Aero. Sci.*, **21**, 1954, 91-108.

[4] DeGraaff, D.E. and Eaton J.K., Reynolds-number scaling of the flat-plate turbulent boundary layer, *J. Fluid Mech.*, **422**, 2000, 319–346.

[5] Harun, Z., Kulandaivelu, V., Nugroho, B., Khashehchi, M., Monty, J.P. and Marusic, I., Large scale structures in an adverse pressure gradient turbulent boundary layer in *8th Int. Sym. on Engineering Turbulence Modelling and Measurements: ETMM8*, 2010, 183–194.

[6] Hutchins, N. and Marusic, I., Large-scale influences in near-wall turbulence, *Phil. Trans. R. Soc. A*, **365**, 2007, 1–28.

[7] Hutchins, N., Nickels, T.B., Marusic, I., and Chong, M.S., Hot-wire spatial resolution issues in wall-bounded turbulence, *J. Fluid Mech.*, **635**, 2009, 103-136.

[8] Jones M.B., Marusic, I., and Perry, A.E., Evolution and structure of sink flow turbulent boundary layer, *J. Fluid Mech.*, **422**, 2001, 1–27.

[9] Lee, J.H. and Sung, H.J., Effects of an adverse pressure gradient on a turbulent boundary layer, *Intl. J. Heat Fluid Flow*, **29**, 2008,568–578.

[10] Marusic, I., and Perry, A.E., A wall-wake model for the turbulence structure of boundary layers. Part 2. Further experimental support, *J. Fluid Mech.*, **298**, 1995, 389–407.

[11] Nagano, Y., Tagawa, M., and Tsuji, T., Effects of adverse pressure gradients on mean flows and turbulence statistics in a boundary layer, *Turbulent Shear Flows 8, Springer, Berlin*, **8**, 1992, 7–21.

[12] Nagano, Y., Tsuji, T., and Houra, T., Structure of turbulent boundary layer subjected to adverse pressure gradient, *Int. J. Heat Fluid Flow*, **19**, 1998, 563–572.

[13] Ng, H.C.H., Marusic, I., Monty, J.P., Hutchins, N., and M. s. Chong, Oil film interferometry in high Reynolds number turbulent boundary layers, *Australasian Fluid Mechanics Conference*, **16**, 2007, 807–814.

[14] Skåre, P.E., and Krogstad, P.- Å., A turbulent equilibrium boundary layer near separation, *J. Fluid Mech.*, **272**, 1994, 319–348.